Frequency dependent seismic anisotropy due to fractures: Fluid flow versus scattering

Alan F. Baird[1], **J.-Michael Kendall**[1], **Doug A. Angus**[2]

[1] *University of Bristol, School of Earth Sciences, Bristol, United Kingdom,*

alan.baird@bristol.ac.uk, gljmk@bristol.ac.uk

[2] *University of Leeds, School of Earth and Environment, Leeds, United Kingdom,*

d.angus@leeds.ac.uk

(January 2, 2013)

Running head: **Frequency dependent anisotropy**

ABSTRACT

Anisotropy is a useful attribute for the detection and characterization of aligned fracture sets in petroleum reservoirs. Unfortunately, many of the traditional effective medium theories for modeling the seismic properties of fractured rock are insensitive to the size of the constituent fractures. For example, the same pattern of anisotropy may be produced by a high concentration of small, stiff cracks; or by a lower concentration of large, compliant fractures. The distinction between these models is important for assessing permeability anisotropy, as fluid flow is dominated by the largest fractures. One method to gain further insight is through the analysis of frequency dependent shear wave splitting in microseismic data, as fracture compliance is frequency dependent, and microseismic data are relatively rich in frequency content. Here we compare two potential mechanisms causing frequency dependent compliance of fractures: (1) squirt flow in fractured porous rock, and (2) wave scattering over rough fractures. Both models show a sensitivity to

average fracture size or compliance of the constituent fractures, and thus provide a potential means to differentiate between anisotropy produced by small cracks or large fractures. We use both mechanisms to model frequency dependent anisotropy data obtained from a fractured gas reservoir, and invert for fracture parameters. Under certain conditions the squirt-flow mechanism can cause significant frequency dependence in the microseismic band. However, the model is highly sensitive to the empirically derived mineral-scale relaxation time which is poorly known and requires laboratory measurements to constrain. Conversely, producing a similar frequency response using the scattering model requires implausible fracture parameters, therefore the squirt-flow model appears to be the most likely mechanism for microseismic applications. At higher frequencies, however, scattering may become more significant. Care should be taken when upscaling ultrasonic laboratory results for field-scale problems, as different mechanisms may be at play within different frequency bands.

INTRODUCTION

Large fractures within petroleum reservoirs often significantly enhance permeability and consequently increase production. While seismic studies lack the resolution required to directly image individual fractures, the presence of aligned fracture sets may produce seismic anisotropy which can be used as a means to characterize the reservoir (e.g. Lynn and Thomsen, 1990; Hall and Kendall, 2003). In addition to fractures there are several other mechanisms which may contribute to the anisotropy of sedimentary rocks, and therefore must be considered. For example, there could be anisotropy related to the rock fabric, such as the preferred alignment of intrinsically anisotropic minerals (e.g. Vernik and Nur, 1992; Valcke et al., 2006; Kendall et al., 2007), or the periodic layering of contrasting lithologies (e.g. Backus, 1962); additionally there may be a stress sensitive contribution to the anisotropy resulting from the alignment of grain-scale microcracks (e.g. Zatsepin and Crampin, 1997; Hall et al., 2008; Verdon et al., 2008). The problem of distinguishing between the different sources of anisotropy can be helped by making some simplifying assumptions about their respective symmetry and orientation. For instance, the fabric of sedimentary rocks is typically aligned horizontally, which produces an anisotropy system with a vertical axis of symmetry (vertical transverse isotropy, VTI); whereas cracks and fracture sets are often vertical or steeply dipping, producing horizontal transverse isotropy (HTI). The combined effect produces a bulk anisotropy with orthorhombic symmetry (e.g. Tsvankin, 1997; Grechka et al., 1999), which can be interpreted in terms of the relative contribution of the fabric and fractures (e.g. Verdon et al., 2009; Wuestefeld et al., 2011).

Distinguishing between anisotropy produced by cracks, which we define as grain-scale features, and larger fractures with lengths on the order of centimeters to meters, is much more difficult

to unravel. The effect of a fracture/crack set on the overall elasticity can be considered as a perturbation to the compliance tensor. The compliance tensor is used rather than the stiffness tensor because it assumes continuity of stress, but strain may be discontinuous. This is appropriate for modeling fractured rock, as fractures represent discontinuities in displacement. The overall strain due to an stress will be the sum of the strains in the rock matrix and fractures. This is calculated by simply adding the excess compliance tensor of the fractures, $\mathbf{S^f}$, to the compliance tensor of the background rock. $\mathbf{S^f}$ has the form (Schoenberg and Sayers, 1995):

$$\mathbf{S^f} = \begin{bmatrix} Z_N & 0 & 0 & 0 & 0 & 0 \\ 0 & 0 & 0 & 0 & 0 & 0 \\ 0 & 0 & 0 & 0 & 0 & 0 \\ 0 & 0 & 0 & 0 & 0 & 0 \\ 0 & 0 & 0 & 0 & Z_T & 0 \\ 0 & 0 & 0 & 0 & 0 & Z_T \end{bmatrix} \tag{1}$$

where Z_N and Z_T are the excess normal and tangential compliances of the crack/fracture set, respectively (see Table for a list of symbols used in the paper). However, excess compliance can come in the form of a few large compliant fractures, or by a higher concentration of smaller stiff fractures or microcracks (Figure 1). Most of the classic attempts to model fracture-induced anisotropy (e.g. Hudson, 1981; Thomsen, 1995) are insensitive to fracture size, but the distinction between these end-members can have significant implications for production, as fluid flow is generally dominated by the largest fractures.

[Figure 1 about here.]

It has been shown through laboratory experiments that the effective dynamic compliance of

grain-scale microcracks (e.g. Dvorkin et al., 1995) and sample-scale fractures (e.g. Pyrak-Nolte and Nolte, 1992; Biwa et al., 2007) are frequency dependent. While these experiments are typically done at ultrasonic frequencies, recent reportings of frequency dependent anisotropy within fractured petroleum reservoirs (e.g. Liu et al., 2003; Maultzsch et al., 2003; Al-Harrasi et al., 2011b) suggest the effect may be observed at seismic exploration frequencies as well. The two most likely models to explain frequency dependent fracture compliance are: (1) a squirt-flow mechanism, involving wave-induced fluid flow in fractured porous rocks (e.g. Chapman, 2003) and (2) a scattering mechanism, involving waves crossing rough fractures with inhomogeneous compliance distributions (e.g. Pyrak-Nolte and Nolte, 1992). While their underlying mechanisms differ, both models are sensitive to properties of the individual component fractures (such as average size or compliance) and thus provide a potential means to distinguish between the end-members in Figure 1. However, if we wish to use frequency dependent anisotropy to invert for these properties, we need to understand the relative importance of each mechanism within the frequency band of interest.

Many techniques are available to estimate seismic anisotropy using conventional seismics; for example, through the detection of azimuthal variations in normal moveout velocities (Tsvankin and Thomsen, 1994; Alkhalifah, 1997; van der Baan and Kendall, 2002) and reflection amplitudes (Lynn and Thomsen, 1990; Hall and Kendall, 2003; Sayers and den Boer, 2011), or through shear wave splitting of P-S converted waves (Ata and Michelena, 1995; Gaiser et al., 2002). However, many of these techniques occur over a relatively narrow frequency bands ($\sim$10–50 Hz), making the detection of frequency dependent effects difficult. An alternative approach is to estimate shear-wave splitting from microseismic events, which are comparatively rich in frequency content ($\sim$10–500 Hz). Microseismic monitoring offers an additional advantage that instruments are often deployed in downhole arrays such that the ray paths (and therefor the measured anisotropy) are entirely contained within

the region of interest.

Shear-wave splitting provides an unambiguous indication of anisotropy. As a shear-wave passes through an anisotropic medium it will split into two orthogonally polarized waves traveling at different velocities. The polarization of the fast wave (ϕ) and the delay between wave arrivals (δt) can be used to characterize the anisotropy along the ray path. The delay time is often normalized by the path length to express anisotropy as a percentage difference in velocity between the fast and slow waves (δ_{V_S}). To estimate frequency dependent anisotropy, the waveform is first filtered into different frequency bands and then splitting parameters estimated for each band. Al-Harrasi et al. (2011a,b), employed this technique to assess frequency dependent anisotropy using a microseismic dataset from a fractured limestone gas field in Oman. They found clear and strong evidence of frequency dependence with anisotropy decreasing with increasing frequencies. Al-Harrasi et al. (2011b) were able to model the data using the squirt-flow theory of Chapman (2003), however, in doing so they neglect other mechanisms, such as scattering, that may be contributing to the frequency dependence.

Here we review the main potential contributors to frequency dependent anisotropy related to fractures, namely the squirt-flow model and the scattering model, to better understand their relative importance within the microseismic frequency band. For the squirt-flow mechanism we use the model of Chapman (2003), and for the scattering mechanism we generalize the model proposed by Pyrak-Nolte and Nolte (1992) and extend it for use with field scale fractures.

[Table 1 about here.]

MECHANISM 1: SQUIRT-FLOW IN FRACTURED POROUS ROCK

It has long been recognized that although velocities of saturated rocks can be accurately predicted by Biot-Gassman theory at low frequencies, they typically underestimate velocities at high frequencies. This discrepancy can be explained with the concept of squirt-flow, which considers local pressure gradients arising from heterogeneity in the pore space (e.g. O'Connell and Budiansky, 1977; Dvorkin et al., 1995). Different elements of the pore space will respond differently to seismic waves. While a pore that is approximately spherical in shape will be quite stiff and resistant to compression, a low aspect ratio microcrack will be very compliant. Because of this excess compliance a rock whose porosity is made up of randomly oriented microcracks will have lower seismic velocities than one with more spherical or equant pores. This additional compliance, however, is also dependent on saturating fluids. While a drained crack is very compliant, one that is isolated and filled with a relatively incompressible fluid will be very stiff. The concept of squirt-flow arises when the pore space is composed of both spherical pores and microcracks. As a wave passes the cracks will compress more than the pores, producing a local pressure gradient and causing the fluid to "squirt" out of the cracks. This allows cracks to effectively drain, and remain compliant, despite being fluid saturated. However, the transfer of fluids does not occur instantaneously, a small amount of time is required for the pressures to fully equalize, which produces a frequency dependent effect when exposed to an oscillatory stress field like a seismic wave. The cracks will only remain compliant if there is sufficient time within a single wave period for the cracks to fully drain and refill. At high frequencies the fluid is effectively trapped in the cracks which then appear stiff, increasing the overall seismic velocities.

Between the low and high frequency end-members, there is a transition zone where pressure

equalization is only partially achieved. This is the range where maximum velocity dispersion and attenuation occurs. The central frequency of this transition zone for an unfractured rock is often referred to as the mineral scale "squirt-flow frequency," ω_m, with the associated relaxation time, $\tau_m = \omega_m^{-1}$. τ_m is empirically derived but is found to be proportional to the viscosity of the saturating fluid, and inversely proportional to the permeability of the host rock (Chapman et al., 2003a). Laboratory measurements on reservoir rocks typically find that the transition frequency lies within the ultrasonic band, much higher than frequencies typically encountered in the field (Thomsen, 1995). As such, the low frequency end-member is often assumed for field studies.

Most traditional squirt-flow models only consider heterogeneity of the grain scale porosity, which is appropriate for the laboratory samples where tests are carried out. However, field scale problems often include much larger fractures, which are not addressed in many of the theories. The multi-scale squirt-flow model of Chapman (2003) extends the models to include larger-scale fractures in addition to grain-scale microcracks and pores. For simplicity it is assumed that the microcracks and fractures share a common shape and aspect ratio, and that there is fluid communication between the fractures and the porosity, but not between fractures directly. This results in an additional relaxation time parameter associated with the fluid response of the fractures, τ_f,

$$\tau_f = \frac{a_f}{\zeta}\tau_m, \tag{2}$$

where a_f is the average fracture radius, and ζ is the average grain size. This larger relaxation time is a consequence of the fractures having a greater ratio of volume to surface area than the microcracks, thus requiring a longer time to drain. This introduces the potential of pushing frequency dependent compliance down into the seismic frequency range. In the case of aligned fractures this should result in observable frequency dependent anisotropy.

The squirt-flow model of Chapman (2003) does not explicitly calculate the fracture compliances, rather it solves for the full anisotropic stiffness tensor directly. However, we can calculate the effective fracture compliances by subtracting the isotropic background compliance from the full anisotropic compliance tensor using the method of Schoenberg and Sayers (1995) (see appendix A for further details). Figure 2 shows predicted normal and tangential compliances as a function of frequency for several different fracture sizes. The model assumes the properties of the N-A carbonate gas reservoir of Al-Harrasi et al. (2011b), with background velocities of $V_P = 2800$ m/s, $V_S = 1470$ m/s, and a density of $\rho = 2400$ kg/m^3. Porosity is taken to be 0.1, with an assumed mineral scale relaxation time of $\tau_m = 9.5 \times 10^{-7}$ s. Tangential compliance shows no frequency dependence, as a tangential displacement across a fracture does not produce a volume change, so additional fluid flow is not induced. Normal compliance, however, is strongly frequency dependent. At low frequencies the fracture will drain when compressed, and appear very compliant, while at high frequencies the fluid will be trapped resulting in a stiffer fracture. As expected the band of frequency dependence is sensitive to the fracture size.

[Figure 2 about here.]

MECHANISM 2: SCATTERING ON ROUGH FRACTURES

A second potential mechanism to explain frequency dependent compliance is wave scattering. Here, rather than represent fractures as low-aspect ratio ellipsoidal inclusions as was done in the squirt-flow model, we use displacement discontinuity theory (Schoenberg, 1980; Pyrak-Nolte et al., 1990). This treats fractures as planar interfaces between two half-spaces with imperfect contact. Traction across the surface is continuous, while displacement is discontinuous and proportional to the fracture

compliances. For a planar interface with normal in the x_1 direction the displacement discontinuity is

$$\Delta u = \begin{bmatrix} B_N & 0 & 0 \\ 0 & B_T & 0 \\ 0 & 0 & B_T \end{bmatrix} \mathbf{t}, \tag{3}$$

where B_N and B_T are the normal and tangential fracture compliances respectively, and $\mathbf{t}$ is the traction. Unlike Z_N and Z_T which describe the equivalent medium compliance of a full fracture set and have dimension 1/stress, B_N and B_T are the compliances of the individual fracture, with dimension length/stress. The two different types of compliance can be related through the equation

$$Z_{N,T} = \frac{B_{N,T}}{H}, \tag{4}$$

where H is the effective fracture spacing. Thus fracture-sets with different individual fracture compliances can have the same equivalent medium compliance provided their spacing is appropriately scaled.

Displacement discontinuity theory can be used to predict transmission coefficients for waves crossing a fracture with uniform compliance. For a wave propagating normal to a fracture the transmission coefficient is (Schoenberg, 1980)

$$T(B_{N,T}, \omega) = \left(1 - \frac{i\omega\rho V_{P,S} B_{N,T}}{2}\right)^{-1}, \tag{5}$$

where ω is the angular frequency, ρ is the density of the matrix rock, $V_{P,S}$ is the velocity of the wave in question (V_P or V_S) and $B_{N,T}$ is the compliance of the fracture. B_N should be used for P-wave transmission and B_T for S-waves. In general the fracture acts as a low-pass filter, with characteristic cut-off frequency

$$\omega_c = \frac{2}{\rho V_{P,S} B_{N,T}}. \tag{6}$$

It follows that fractures with different compliances will have different cut-off frequencies. In laboratory studies the dynamic fracture compliance can be estimated by matching experimentally determined transmission coefficients against theoretical values predicted by the displacement discontinuity model. Equation 5 can easily be inverted for compliance to give

$$B_{N,T} = \frac{2\sqrt{1-|T|^2}}{\omega \rho V_{P,S}|T|}. \tag{7}$$

Local variations in compliance

One of the underlying assumptions of equation 5 is that the compliance of the fracture is homogeneous over the area sampled by the passing wave. In reality this is likely untrue, as fracture surfaces are made up of a complex arrangement of asperities in contact separated by void spaces of various shapes and sizes, and are therefore strongly heterogeneous. Pyrak-Nolte and Nolte (1992) argued that such a fracture could be modeled as a planar contact with a heterogeneous distribution of local compliances and that such an arrangement should produce an apparent frequency dependent compliance.

The apparent frequency dependence arises due to spatial averaging of transmission coefficients over the fracture. Since different portions of the fracture have different local compliances, they will also have different characteristic cut-off frequencies (ω_c in equation 6). For a given frequency, only portions of the fracture with ω_c higher than that of the propagating wave will transmit the signal, while portions with lower ω_c will tend to reflect or backscatter the signal (Figure 3). At very low frequencies ($\omega \to 0$) all portions of the fracture would be expected to transmit the wave. As frequency increases the more compliant portions will begin to scatter the signal (since $\omega_c \propto 1/B_{N,T}$, equation 6), and the transmitted wave will only sample the stiffer portions leading to an apparent

decrease in compliance.

[Figure 3 about here.]

To determine the apparent dynamic compliance of a real fracture we must first calculate the average transmission coefficient over the fracture surface S which can be expressed as

$$T(B_{app}(\omega), \omega) = \frac{1}{|S|} \int_S T(B_{loc}, \omega)\, dS, \tag{8}$$

where B_{loc} is the spatially varying local compliance, and the function $T(B_{loc}, \omega)$ is given by equation 5. The use of equation 8 requires knowledge of the spatial variation of local compliance on the fracture surface. Alternatively the above integral can be expressed as

$$T(B_{app}(\omega), \omega) = \int_0^\infty T(B_{loc}, \omega) f(B_{loc})\, dB_{loc}, \tag{9}$$

where $f(B_{loc})$ is a probability distribution function describing local compliance (Biwa et al., 2007). This averaged transmission coefficient can then be substituted into equation 7 to give an apparent frequency dependent fracture compliance

$$B_{Napp,Tapp}(\omega) = \frac{2\sqrt{1 - |T(\omega)|^2}}{\omega \rho V_{P,S} |T(\omega)|}. \tag{10}$$

Pyrak-Nolte and Nolte (1992) and Biwa et al. (2007) were able to use this model to explain frequency dependent compliance for stiff fractures in laboratory settings at ultrasonic frequencies. It remains unresolved whether similar frequency dependence may be expected for larger, reservoir-scale fractures at exploration seismic frequencies.

Fracture model

Hudson et al. (1997) derived expressions to estimate the compliance of fractures modeled as in-

terfaces between two surfaces that are not in perfect contact but are characterized as a planar distribution of welded regions. The model assumes that wavelengths are long compared to the length scale of the welded regions, and that the relative area of welded contact between the surface is small. For a drained fracture the ratio of normal to tangential compliance was found to be (Liu et al., 2000):

$$\frac{B_N}{B_T} = \frac{1-\nu}{1-\nu/2}. \tag{11}$$

where ν is the Poisson's ratio of the rock matrix. Additionally, it was found that for a fixed proportion of contact area the magnitudes of the fracture compliances (both B_N and B_T) are proportional to the average size of the contact points. A fracture with many small and closely spaced asperities in contact will be much stiffer than a fracture with more widely spaced larger contact zones. Worthington and Lubbe (2007) compiled a list of published estimates of fracture compliance from various scales, and noted that compliance tended to increase with increasing fracture size (Figure 4). They argued that because of the fractal nature of surface roughness (e.g. Brown and Scholz, 1985), the average size of the contact zones across a rough fracture may act as a proxy for fracture size, thus explaining the apparent increase in compliance.

[Figure 4 about here.]

Unfortunately equations of Hudson et al. (1997) are insufficient to model frequency dependent compliance as they provide only single value estimates of compliance for the whole fracture. Since the derivation of the equations assumed a long wavelength, the results may be thought of as the low frequency limit of equation 10. That is; as $\omega \to 0$, $|T| \to 1$, and equation 10 reduces to a simple spatial average of the local compliances with equal weighting. We denote these low frequency average compliances B_{N0}, and B_{T0} (with their associated effective media compliance counterparts

Z_{N0} and Z_{T0}). In order to model frequency dependence, the model must be modified to allow for variations in compliance within the fracture. This can be achieved by imposing an appropriate probability distribution function for local compliances.

Here we make the assumption that local compliance is log-normally distributed over a fracture. This is based on the recognition that aperture distributions of natural rough walled fractures are often found to be approximately log-normal (e.g. Gale, 1987; Nolte and Pyrak-Nolte, 1991; Keller, 1998). Strictly-speaking, compliance expressions derived by Hudson et al. (1997) are not explicitly dependent on the fracture aperture, but on the size and distribution of the welded regions. However, compliance is also dependent on the rate of formation of new contact area due to an increase in normal stress (Pyrak-Nolte and Morris, 2000), which is directly dependent on the local aperture distribution.

That is, the fracture aperture, h, will have a probability distribution function in the form:

$$f(h) = \frac{1}{Sh\sqrt{2\pi}} \exp\left\{-\frac{(\ln(h) - M)^2}{2S^2}\right\} \tag{12}$$

where M and S are the location and scale parameters, respectively, of the log-normal distribution. This can be related to the mean aperture, $\langle h \rangle$, and its standard deviation, σ_h, through the expressions:

$$S^2 = \ln\left[1 + \left(\frac{\sigma_h}{\langle h \rangle}\right)^2\right], \tag{13}$$

$$M = \ln\langle h \rangle - \frac{1}{2}S^2. \tag{14}$$

Figure 5 shows examples of log-normal distributions of fracture aperture. Each distribution is normalized to have a mean value of 1, but with different relative roughness, $\frac{\sigma_h}{\langle h \rangle}$, which controls the "skewness" of the distribution. For low values of roughness the distribution is approximately

normal, which is applicable for relatively smooth fractures. As roughness increases the distribution becomes progressively skewed towards low apertures, but with a long tail. For simplicity we assume, due to the fractal nature of fracture roughness, that the standard deviation of aperture will scale with the mean aperture such that the relative roughness $\frac{\sigma_h}{\langle h \rangle}$ remains constant.

[Figure 5 about here.]

Once a probability distribution function of stiffness (or compliance) is estimated, then an average transmission coefficient for a given frequency can be calculated using equation 9, which can then be substituted into equation 10 to calculate the apparent compliance of the fracture. In practice the average transmission coefficient from equation 9 is estimated using a Monte Carlo simulation, where the integral is replaced by the summation

$$T(Z(\omega), \omega) = \frac{1}{N} \sum_{\ell=1}^{N} T(B_\ell, \omega), \tag{15}$$

where N is an arbitrary large number. B_ℓ is a fracture compliance randomly sampled from the probability distribution function of local compliances $f(B_{loc})$, and $T(B_\ell, \omega)$ is calculated using equation 5.

[Figure 6 about here.]

Figure 6 shows predicted frequency dependent compliances due to scattering for various values of mean compliance (6a) and relative roughness (6b) for a model with background velocities of $V_P = 2800$ m/s, $V_S = 1470$ m/s, and a density of $\rho = 2400$ kg/m^3. The frequency band over which the frequency dependence is observed is strongly controlled by the mean compliance of the fractures. Much like in the squirt-flow model, a fracture set produced by larger, more compliant

fractures will show frequency dependence at lower frequencies than stiff fractures. Increasing the relative roughness has the effect of broadening the frequency band affected and increasing the magnitude of the change in compliance. Unlike the squirt-flow model, here both the normal and tangential compliances show frequency dependence. Although the overall compliance decreases, the normal to tangential compliance ratio shows very little variation.

PREDICTED SHEAR-WAVE SPLITTING

Since the magnitude of shear-wave splitting produced by a fracture set is proportional to its total excess compliance, frequency dependent compliance will produce frequency dependent shear-wave splitting. To model shear wave splitting we first must estimate an effective medium stiffness tensor incorporating both the background rock properties and the aligned fracture set. For the squirt-flow model this is calculated directly (see appendix A and Chapman, 2003, for more detail), however for the scattering model this must be constructed. First the fracture compliances (B_N, and B_T) for a given frequency are estimated using the methodology described in the fracture model section, then effective media fracture compliances (Z_N, and Z_T) for a given fracture spacing, H, are calculated using equation 4. These are used to produce the fracture set excess compliance tensor $\mathbf{S^f}$ (equation 1), which is added to the background rock compliance, $\mathbf{S^b}$, following the method of Schoenberg and Sayers (1995). This is then inverted to produce an effective stiffness tensor, $\mathbf{C^{eff}}$:

$$\mathbf{C^{eff}} = (\mathbf{S^b} + \mathbf{S^f})^{-1}. \tag{16}$$

Once the stiffness tensor is constructed the phase velocities; V_P, V_{S1} and V_{S2}, for a given propagation direction are computed by solving the Christoffel equation. Shear wave splitting is then calculated

using:

$$\delta V_S = 100 \frac{V_{S1} - V_{S2}}{(V_{S1} + V_{S2})/2}. \tag{17}$$

The magnitude of the frequency dependence will depend on the wave propagation direction relative to the fracture-set orientation.

We choose parameters for both models that will produce frequency dependence within the microseismic frequency band (∼10–500 Hz). For the squirt-flow model we use a fracture size of 1 m, a fracture density of 0.025 and a relaxation time of $\tau_m = 9.5 \times 10^{-7}$ s. For the scattering model we use a mean fracture compliance of $B_{T0} = 10^{-10}$ m/Pa, a roughness parameter of $\frac{\sigma_h}{\langle h \rangle} = 1.0$, and an average fracture spacing of $H = 10$ m (producing a mean effective medium compliance of $Z_{T0} = 10^{-11}\text{Pa}^{-1}$). Figure 7 shows the predicted frequency dependent shear wave splitting from each model for a range of different wave propagation directions relative to the fracture orientation. For waves propagating normal to the fractures (azimuth = 0°) both models predict no splitting. Both models show the maximum splitting magnitude for wave propagating parallel to the fractures (azimuth = 90°), but with a very different frequency response. For this propagation direction, splitting is controlled only by the tangential compliance, which in the case of the squirt-flow model is frequency independent since it is not affected by fluid compressibility (Figure 2). Conversely, for the scattering model the tangential compliance is strongly frequency dependent (Figure 6), resulting in observable frequency dependent anisotropy. It should be noted that our model assumes perfectly aligned fractures, an arrangement which is unlikely to occur in nature. Tod (2001) showed that a 'nearly aligned' fracture set can behave differently from a perfectly aligned set, and we suspect that a natural fracture set would show some frequency dependence for fracture parallel propagation.

[Figure 7 about here.]

Both Z_N and Z_T play a role in the splitting for waves propagating at oblique angles to the fracture, with Z_N becoming increasingly important as you approach the fracture normal. In the scattering model both compliances are affected in a similar way, therefore we see only subtle variations in the frequency dependence for different propagation directions (other than a decrease in overall splitting magnitude as you approach the fracture normal). For the squirt-flow model, however, since Z_N and Z_T diverge substantially at higher frequencies, we see a large azimuthal variation in frequency dependent anisotropy. In general δV_S decreases as frequency increases, except for certain propagation directions closer to the fracture normal where splitting decreases until it reaches zero, and then begins to increase again (propagation directions of 15°, 30°, and 45° in Figure 7a). The decrease and then increase in δV_S is also accompanied by a 90° flip in fast wave polarization and this is due to an azimuthal and frequency dependent slowness surface singularity developing (i.e. when the fast and slow shear waves have the seem wave speed). This phenomenon will only occur if the ratio of normal to tangential compliance, Z_N/Z_T, is sufficiently low, and can possibly be used as a means to distinguish between the models in certain situations.

Sensitivity analysis of scattering model

Here we use synthetic modeling of shear wave splitting to test the sensitivity of the each of the input parameters of the scattering model (See Al-Harrasi et al., 2011b, for a sensitivity analysis of the squirt-flow model). For the base model we assume average background V_P and V_S velocities of 2800 m/s and 1470 m/s, respectively and unless stated otherwise, an average individual fracture tangential compliance of $B_{T0} = 10^{-10}$ m/Pa, equivalent-media compliance of $Z_{T0} = 10^{-11}$ Pa^{-1}, relative roughness of $\frac{\sigma_h}{\langle h \rangle} = 1.0$ and a wave propagation direction of 75° from the fracture normal. Figure 8 shows model sensitivity to each of these input parameters.

[Figure 8 about here.]

As expected, the amount of frequency dependence is strongly affected by the average compliance of the individual fractures (B_{T0}, Figure 8a). For this example fractures with compliances on the order of 10^{-10} m/Pa and higher may produce observable FDA at microseismic frequencies, however stiffer fractures show little frequency dependence. It should be noted that while B_{T0} is varied, the fracture spacing, H, is also varied as per equation 4 to maintain a constant mean effective-media compliance Z_{T0}.

Figure 8b shows the effect of changing Z_{T0} by varying the spacing of fractures with a fixed B_{T0}. Here the main effect is to increase the magnitude of splitting with higher values of Z_{T0}, yet the frequency dependence is not strongly affected. Within the Carbonate field of the data-set, although some SWS measurements showed anisotropy as high as 18%, most measurements ranged between 0–10% (Al-Harrasi et al., 2011a), thus Z_{T0} is likely lower than 10^{-10} Pa^{-1}.

The effect of relative roughness on the frequency response is shown in Figure 8c. As expected a greater amount of frequency dependence is observed as roughness increases. It is not clear how high a roughness parameter may naturally occur in fractures, however Zimmerman and Main (2003) shows data on hydraulic transmissivities of simulated fractures which varied in roughness between 0.1–2.

Figure 8d shows the effect of varying the propagation direction relative to the fracture orientation. Here the main effect is a shift in the magnitude of splitting, with maximum anisotropy observed parallel to the fracture (90°) and no splitting normal to the fracture (0°).

FRACTURE INVERSION EXAMPLE

Although the squirt-flow and scattering models differ in the underlying mechanism producing the frequency dependent compliance (and anisotropy), they are similar in that they are both sensitive to the average size or compliance of the constituent fractures. Within the microseismic frequency band both models predict high frequency dependence for large open fractures, but not for smaller stiff fractures. Thus both models can potentially be used to help differentiate between fracture- and crack-induced anisotropy.

The question of which mechanism will dominate at microseismic frequencies is more difficult. To better illustrate the possible contributions of each mechanism we attempt to invert fracture properties using an example of frequency dependent shear-wave splitting data taken from the study of Al-Harrasi et al. (2011b). In this study and their companion paper (Al-Harrasi et al., 2011a), the authors characterize a fractured carbonate gas field in Oman using both broadband and frequency dependent shear-wave splitting analysis derived from microseismic data. The events were recorded using oriented 3-component geophones placed in downhole arrays. Splitting analysis was restricted to source/receiver pairs located within the same rock unit, such that anisotropy along the ray path may be attributed entirely to a single formation and errors due to heterogeneity could be minimized. For each 3-componant waveform, splitting parameters ϕ (the polarization of the fast shear-wave) and δt (the time delay between the fast and slow shear-waves) are estimated using the approach of Wuestefeld et al. (2010). First, the three component data are rotated from its acquisition geometry into rayframe coordinates (the longitudinal component which maximizes the P-wave energy, and the orthogonal SH and SV components which contain the S-wave energy). A window is placed around the S-arrival. If the wave passes through an isotropic medium the particle

motion in the SH-SV plane within the window should be approximately linear, however if it passes through an anisotropic medium the S-wave will begin to split resulting in a more elliptical particle motion. The analysis performs a grid search over all possible fast polarizations and delay times to find splitting parameters that best linearize the particle motion, thus removing the observed effects of splitting. The analysis is done using 100 windows around the S-arrival, and a cluster analysis is used to infer the stability of the solution (Teanby et al., 2004). The technique also provides an objective measure of the quality of the measurement (see Wuestefeld et al., 2010, for details).

Only waveforms which produced high quality splitting measurements using the broadband data were used for frequency dependent analysis. To do this Al-Harrasi et al. (2011b) first filtered the waveforms using a series of narrow frequency bands of 1 octave width (i.e 10-20 Hz, 15-30 Hz, 20-40 Hz, 30-60 Hz... etc). The splitting approach and associated quality control of Wuestefeld et al. (2010) is then applied to the filtered waveforms to estimate the splitting parameters. If a single waveform does not produce a sufficient number of high quality measurements to clearly show the frequency dependence, then it is not used. The time delay, δt, is then normalized by the path length to estimate percentage difference in the velocity of the fast and slow waves, δV_S. The data plotted in Figures 9 and 10, show an example of good quality frequency dependent splitting results obtained by Al-Harrasi et al. (2011b) from a single waveform within the N-A gas reservoir. The estimated magnitude of anisotropy is plotted against the dominant frequency of each filtered waveform.

In order to model frequency dependent splitting using real data we assume that the anisotropy is the result of a single set of aligned fractures embedded within a homogeneous isotropic medium. These conditions are unlikely to be strictly true, reservoir rocks often show some degree of anisotropy

due to rock fabric, however, in carbonate rocks intrinsic anisotropy is generally found to be negligible Wang (2002). Heterogeneity along the ray-path is not considered, however, we believe that it is minimized by considering only source/reciever pairs within the same rock unit. We note that in our inversions we make no prior assumptions about fracture dip. Fracture orientation is defined as the angle between the ray-path and the fracture normal, which can be achieved by changing either strike or dip. This is in contrast to the inversions of Al-Harrasi et al. (2011b), which assumed horizontal propagating waves and a fixed dip angle.

Of the two freqency dependent anisotropy mechanisms described the squirt-flow model has many more variables controlling the frequency band most affected. In addition to fracture size, the frequency response is also very sensitive to fluid and rock properties such as viscosity and permeability, which control the mineral-scale relaxation time, τ_m. Al-Harrasi et al. (2011b) applied an inversion scheme to solve for squirt-flow fracture parameters which best fit the data. We have reproduced their results, which yielded an estimated fracture radius of 2.75 m in Figure 9. For the inversion they used an assumed τ_m of 9.5×10^{-7} s. However, this was not derived from laboratory measurements on the field rocks, instead the technique of Chapman et al. (2003a) was used to estimate τ_m from published data which used different rocks and fluid types. Extrapolation of τ_m from one rock type to another can lead to significant and unquantifiable error. The dashed lines in Figure 9 show that increasing and decreasing τ_m by an order of magnitude has a substantial effect on the predicted frequency response. The roles of fracture size and τ_m in controlling the frequency response are governed by equation 2 which shows that there is a one-to-one trade-off in their respective accuracies. If the estimated τ_m is an order of magnitude too high, then the apparent fracture size will be an order of magnitude too low. Clearly, care must be taken when interpreting the results of the inversions, as accurate results require detailed laboratory analysis to

constrain the input parameters.

An additional weakness of the squirt-flow model is that it assumes that both cracks and fractures can be modeled with a very simple common shape and aspect ratio. While a simplified circular penny-shaped geometry may be justified for small cracks, it is unlikely that a fracture of this type larger than a few centimeters would remain open at reservoir pressures (Myer, 2000; Worthington, 2008). A more realistic representation would have these larger fractures held open by a number of weld points over their surface, similar to the fractures described in the scattering model. It is likely that this would result in a departure from the model predictions for these larger fractures, although it is unclear how to quantify this divergence.

[Figure 9 about here.]

Conversely the scattering model is not dynamic in nature, but simply the result of waveform averaging over heterogeneous fractures. The band of frequency affected is determined almost entirely by the mean fracture compliance, with the width of the band expanding for rougher fractures (Figure 6).

To test whether a scattering model could produce the frequency dependent anisotropy observed by Al-Harrasi et al. (2011b) we employ an inversion scheme to solve for the best fitting fracture parameters. We perform a grid search over ray azimuth, mean individual fracture tangential compliance (B_{T0}), mean effective-media tangential compliance (Z_{T0}, related to fracture spacing, H, through equation 4), and relative fracture roughness ($\frac{\sigma_h}{\langle h \rangle}$). We pick the combination of parameters which best minimizes the RMS misfit between the observed and modeled data. First we search over a coarse grid (power steps of 10^N for B_{T0} and Z_{T0}, 10° steps for azimuth, and 0.5 steps for $\frac{\sigma_h}{\langle h \rangle}$) to

find the best fitting order of magnitude compliances. We then perform a finer search around the best fitting parameters from the first step.

[Figure 10 about here.]

Figure 10 show the best fit inversion results for the scattering model. Although the model provides a good fit to the data, the parameters are generally less well constrained than the squirt-flow model, and many of them fall outside the range that we would reasonably expect from a fractured reservoir. The best fitting mean fracture compliance, for instance, is 2.6×10^{-9} m/Pa. Comparing this to the admittedly rather sparse compilation of experimental data from Worthington and Lubbe (2007) (Figure 4), we see that most field-scale fractures range in compliance from around 10^{-13}–10^{-11} m/Pa; more than two orders of magnitude lower than our inverted result. While there does exist a single estimate of fracture compliance on the order of 10^{-9} m/Pa, this is from a major fault zone rather than a typical fractured reservoir (Worthington and Hudson, 2000). Additionally this estimate was made based on a possibly faulty assumption that a seismic Q anomaly associated with the fault could be explained by a very low tangential compliance, rather than through some other mechanism (Hobday and Worthington, 2012). As indicated by the sensitivity analysis (Figure 8), a reduction of B_{T0} to levels more in line with experimental data would dramatically reduce the frequency dependence. Similarly, the inferred relative roughness parameter of 3.3 is higher than we would expect, however this parameter is much less constrained.

A further problem with the inversion of Figure 10, is that the inferred fracture spacing is very low (22 cm) given that the individual fracture compliances are similar to "major fault zones". This produces an effective-media compliance of $Z_{T0} = 1.2 \times 10^{-8}$ Pa^{-1}. Although the inverted splitting magnitudes seem reasonable, this is for an inverted propagation direction of just 10° from

the fracture normal, where we would expect low magnitude splitting. The sensitivity analysis (Figure 8b) shows that Z_{T0} this high would produce implausibly high splitting magnitudes for waves propagating close to the strike of the fractures. To address this we performed an additional inversion (not shown) where the wave azimuth was restricted to 90° (fracture parallel). This inversion provided a poorer fit to the data, and yielded a similar fracture compliance ($B_{T0} = 3.16 \times 10^{-9}$ m/Pa), but with a much wider spacing (26 m). While this arrangement is somewhat more reasonable, it still requires implausibly high fracture compliances. Furthermore, very compliant fractures require much larger spacing to produce the same effective medium compliance as stiff fractures (equation 4). Fractured rock can only validly be represented as an effective medium if the fracture spacing is small relative to the seismic wavelength, regardless of which model is used. The fracture spacing required to produce a reasonable effective medium compliance for the scattering model would likely violate this rule for very compliant fractures.

CONCLUSIONS

We have compared two viable mechanisms for frequency dependent anisotropy within fractured reservoirs: (1) The multi-scale squirt-flow model of Chapman (2003), which considers the effect of wave induced fluid flow between fractures and equant pores. (2) A wave scattering model due to fracture roughness, based on the method proposed by Pyrak-Nolte and Nolte (1992). Although the two models differ greatly in their underlying mechanism they both show a similar sensitivity to the average compliance of the component fractures. With large open fractures affecting lower frequency bands than small stiff fractures.

Based on reasonable constraints on maximum fracture compliances expected in field settings,

the frequency dependent effect of scattering is expected to be relatively minor at microseismic frequencies, and can likely be ignored. However, the scattering mechanism may become important at higher frequencies. For example, for cross hole surveys in the kHz range, or for ultrasonic laboratory experiments. A consideration should also be made when upscaling laboratory estimates of dynamic compliance for field-scale problems.

The the squirt-flow model is better suited for explaining frequency dependent anisotropy from microseismic data. However, the model should be applied with the caveat that detailed knowledge of fluid properties and rock matrix permeability are required to constrain results. In particular, an incorrect estimate of the τ_m parameter can lead to significant errors in the inferred dominant fracture size. Nevertheless, the model shows great promise for explaining frequency dependent anisotropy in fractured reservoirs, and even without detailed knowledge of τ_m, may be used to gauge the relative fracture sizes within the same field to potentially identify more highly fractured "sweet spots".

ACKNOWLEDGMENTS

We would like to thank Associate Editor Ivan Vasconcelos, Michael Worthington, and two anonymous reviewers for their constructive comments that helped improve the manuscript. Funding for the work has been provided by the sponsors of the Bristol University Microseismicity Projects (BUMPS) and by the sponsors of the GESER project.

APPENDIX A

SQUIRT-FLOW EQUATIONS

The multi-scale squirt-flow model of Chapman (2003) does not explicitly solve for fracture compliance. Instead it calculates the effective stiffness tensor, $\mathbf{C^{eff}}$, by applying corrections to the isotropic background stiffness tensor, $\mathbf{C^{iso}}$, directly. The expressions for the elements of $\mathbf{C^{eff}}$ are of the form:

$$C^{\mathrm{eff}}_{ijkl} = C^{\mathrm{iso}}_{ijkl} - \phi_{\mathrm{p}} C^{1}_{ijkl} - \varepsilon_{\mathrm{c}} C^{2}_{ijkl} - \varepsilon_{\mathrm{f}} C^{3}_{ijkl}, \tag{A-1}$$

where $\mathbf{C^1}$, $\mathbf{C^2}$, and $\mathbf{C^3}$ are the contributions from pores, grain-scale cracks, and aligned fractures, respectively, and are multiplied by porosity ϕ_{p}, crack density ε_{c}, and fracture density ε_{f}. $\mathbf{C^1}$, $\mathbf{C^2}$, and $\mathbf{C^3}$ are functions of the Lamé parameters, fluid properties, the relaxation time τ_m, fracture radius a_f, and frequency ω. For the precise equations for each component of the stiffness tensor see Chapman (2003). For applications with high porosity and frequencies below the mineral scale squirt-flow frequency, the crack density term in equation A-1 can be neglected (Chapman et al., 2003b).

To estimate the effective media compliances of the fractures, we employ the excess compliance approach of Schoenberg and Sayers (1995) in reverse. In addition to calculating the effective stiffness tensor of the fractures rockmass using equation A-1, we also calculate the equivalent stiffness tensor with the fractures omitted (i.e. only considering the background rock and the porosity, $\mathbf{C^{iso+p}}$). The excess compliance tensor of the fracture set can be estimated by inverting these stiffnesses and subtracting the effect of the background and porosity contributions,

$$\mathbf{S^f} \approx (\mathbf{C^{eff}})^{-1} - (\mathbf{C^{iso+p}})^{-1}. \tag{A-2}$$

$\mathbf{S^f}$ should be approximately in the form of equation 1, such that Z_N and Z_T can be extracted.

REFERENCES

Al-Harrasi, O. H., A. Al-Anboori, A. Wüstefeld, and J.-M. Kendall, 2011a, Seismic anisotropy in a hydrocarbon field estimated from microseismic data: Geophysical Prospecting, **59**, 227–243.

Al-Harrasi, O. H., J.-M. Kendall, and M. Chapman, 2011b, Fracture characterization using frequency-dependent shear wave anisotropy analysis of microseismic data: Geophysical Journal International, **185**, 1059–1070.

Alkhalifah, T., 1997, Velocity analysis using nonhyperbolic moveout in transversely isotropic media: Geophysics, **62**, 1839–1854.

Ata, E., and R. J. Michelena, 1995, Mapping distribution of fractures in a reservoir with ps converted waves: The Leading Edge, **14**, 664–676.

Backus, G. E., 1962, Long-wave elastic anisotropy produced by horizontal layering: Journal of Geophysical Research, **67**, 4427–4440.

Biwa, S., S. Hiraiwa, and E. Matsumoto, 2007, Stiffness evaluation of contacting surfaces by bulk and interface waves: Ultrasonics, **47**, 123–129.

Brown, S. R., and C. H. Scholz, 1985, Broad bandwidth study of the topography of natural rock surfaces: Journal of Geophysical Research, **90**, 12575–12582.

Chapman, M., 2003, Frequency-dependent anisotropy due to meso-scale fractures in the presence of equant porosity: Geophysical Prospecting, **51**, 369–379.

Chapman, M., S. Maultzsch, and E. Liu, 2003a, Some estimates of the squirt-flow frequency: SEG Annual Meeting.

Chapman, M., S. Maultzsch, E. Liu, and X. Li, 2003b, The effect of fluid saturation in an anisotropic multi-scale equant porosity model: Journal of applied geophysics, **54**, 191–202.

Dvorkin, J., G. Mavko, and A. Nur, 1995, Squirt flow in fully saturated rocks: Geophysics, **60**,

97–107.

Gaiser, J., E. Loinger, H. Lynn, and L. Vetri, 2002, Birefringence analysis at emilio field for fracture characterization: First Break, **20**, 505–514.

Gale, J. E., 1987, Comparison of coupled fracture deformation and fluid flow models with direct measurements of fracture pore structure and stress-flow properties: Presented at the 28th US Symposium on Rock Mechanics (USRMS).

Grechka, V., S. Theophanis, and I. Tsvankin, 1999, Joint inversion of P-and PS-waves in orthorhombic media: Theory and a physical modeling study: Geophysics, **64**, 146–161.

Hall, S. A., and J.-M. Kendall, 2003, Fracture characterization at Valhall: Application of P-wave amplitude variation with offset and azimuth (AVOA) analysis to a 3D ocean-bottom data set: Geophysics, **68**, 1150–1160.

Hall, S. A., J.-M. Kendall, J. Maddock, and Q. Fisher, 2008, Crack density tensor inversion for analysis of changes in rock frame architecture: Geophysical Journal International, **173**, 577–592.

Hobday, C., and M. Worthington, 2012, Field measurements of normal and shear fracture compliance: Geophysical Prospecting, **60**, 488–499.

Hudson, J., 1981, Wave speeds and attenuation of elastic waves in material containing cracks: Geophysical Journal of the Royal Astronomical Society, **64**, 133–150.

Hudson, J., E. Liu, and S. Crampin, 1997, The mean transmission properties of a fault with imperfect facial contact: Geophysical Journal International, **129**, 720–726.

Keller, A., 1998, High resolution, non-destructive measurement and characterization of fracture apertures: International Journal of Rock Mechanics and Mining Sciences, **35**, 1037–1050.

Kendall, J.-M., Q. J. Fisher, S. Covey Crump, J. Maddock, A. Carter, S. A. Hall, J. Wookey, S. L. A. Valcke, M. Casey, G. Lloyd, and W. Ben Ismail, 2007, Seismic anisotropy as an indicator

of reservoir quality in siliciclastic rocks: Geological Society, London, Special Publications, **292**, 123–136.

Liu, E., J. Hudson, and T. Pointer, 2000, Equivalent medium representation of fractured rock: Journal of Geophysical Research, **105**, 2981–3000.

Liu, E., J. H. Queen, X. Y. Li, M. Chapman, S. Maultzsch, H. B. Lynn, and E. M. Chesnokov, 2003, Observation and analysis of frequency-dependent anisotropy from a multicomponent VSP at Bluebell-Altamont field, Utah: Journal of Applied Geophysics, **54**, 319–333.

Lynn, H. B., and L. A. Thomsen, 1990, Reflection shear-wave data collected near the principal axes of azimuthal anisotropy: Geophysics, **55**, 147–156.

Maultzsch, S., M. Chapman, E. Liu, and X. Y. Li, 2003, Modelling frequency-dependent seismic anisotropy in fluid-saturated rock with aligned fractures: implication of fracture size estimation from anisotropic measurements: Geophysical Prospecting, **51**, 381–392.

Myer, L., 2000, Fractures as collections of cracks: International Journal of Rock Mechanics and Mining Sciences, **37**, 231–243.

Nolte, D. D., and L. J. Pyrak-Nolte, 1991, Stratified continuum percolation: Scaling geometry of hierarchical cascades: Physical Review A, **44**, 6320–6333.

O'Connell, R. J., and B. Budiansky, 1977, Viscoelastic properties of fluid-saturated cracked solids: Journal of Geophysical Research, **82**, 5719–5735.

Pyrak-Nolte, L. J., and J. P. Morris, 2000, Single fractures under normal stress: The relation between fracture specific stiffness and fluid flow: International Journal of Rock Mechanics and Mining Sciences, **37**, 245–262.

Pyrak-Nolte, L. J., L. R. Myer, and N. G. W. Cook, 1990, Transmission of seismic waves across single natural fractures: Journal of Geophysical Research, **95**, 8617–8638.

Pyrak-Nolte, L. J., and D. D. Nolte, 1992, Frequency dependence of fracture stiffness: Geophysical Research Letters, **19**, 325–328.

Sayers, C. M., and L. D. den Boer, 2011, Characterizing production-induced anisotropy of fractured reservoirs having multiple fracture sets: Geophysical Prospecting. (doi: 10.1111/j.1365-2478.2011.01030.x).

Schoenberg, M., 1980, Elastic wave behavior across linear slip interfaces: The Journal of the Acoustical Society of America, **68**, 1516–1521.

Schoenberg, M., and C. M. Sayers, 1995, Seismic anisotropy of fractured rock: Geophysics, **60**, 204–211.

Teanby, N. A., J.-M. Kendall, and M. Van der Baan, 2004, Automation of shear-wave splitting measurements using cluster analysis: Bulletin of the Seismological Society of America, **94**, 453.

Thomsen, L., 1995, Elastic anisotropy due to aligned cracks in porous rock: Geophysical Prospecting, **43**, 805–829.

Tod, S., 2001, The effects on seismic waves of interconnected nearly aligned cracks: Geophysical Journal International, **146**, 249–263.

Tsvankin, I., 1997, Anisotropic parameters and P-wave velocity for orthorhombic media: Geophysics, **62**, 1292–1309.

Tsvankin, I., and L. Thomsen, 1994, Nonhyperbolic reflection moveout in anisotropic media: Geophysics, **59**, 1290–1304.

Valcke, S. L. A., M. Casey, G. E. Lloyd, J.-M. Kendall, and Q. J. Fisher, 2006, Lattice preferred orientation and seismic anisotropy in sedimentary rocks: Geophysical Journal International, **166**, 652–666.

van der Baan, M., and J.-M. Kendall, 2002, Estimating anisotropy parameters and traveltimes in

the τ-p domain: Geophysics, **67**, 1076–1086.

Verdon, J. P., D. A. Angus, J.-M. Kendall, and S. A. Hall, 2008, The effect of microstructure and nonlinear stress on anisotropic seismic velocities: Geophysics, **73**, D41–D51.

Verdon, J. P., J.-M. Kendall, and A. Wüstefeld, 2009, Imaging fractures and sedimentary fabrics using shear wave splitting measurements made on passive seismic data: Geophysical Journal International, **179**, 1245–1254.

Verdon, J. P., and A. Wüstefeld, 2012, Measurement of the ratio of normal/tangential compliance ratio (Z_N/Z_T) during hydraulic fractures stimulation using shear wave splitting data: Geophysical Prospecting. (accepted).

Vernik, L., and A. Nur, 1992, Ultrasonic velocity and anisotropy of hydrocarbon source rocks: Geophysics, **57**, 727–735.

Wang, Z., 2002, Seismic anisotropy in sedimentary rocks, part 2: Laboratory data: Geophysics, **67**, 1423–1440.

Worthington, M. H., 2008, Interpreting seismic anisotropy in fractured reservoirs: First Break, 57.

Worthington, M. H., and J. A. Hudson, 2000, Fault properties from seismic Q: Geophysical Journal International, **143**, 937–944.

Worthington, M. H., and R. Lubbe, 2007, The scaling of fracture compliance: Geological Society, London, Special Publications, **270**, 73–82.

Wuestefeld, A., O. Al-Harrasi, J. P. Verdon, J. Wookey, and J.-M. Kendall, 2010, A strategy for automated analysis of passive microseismic data to image seismic anisotropy and fracture characteristics: Geophysical Prospecting, **58**, 755–773.

Wuestefeld, A., J. P. Verdon, J.-M. Kendall, J. Rutledge, H. Clarke, and J. Wookey, 2011, Inferring rock fracture evolution during reservoir stimulation from seismic anisotropy: Geophysics, **76**,

WC159–WC168.

Zatsepin, S. V., and S. Crampin, 1997, Modelling the compliance of crustal rock—I. Response of shear-wave splitting to differential stress: Geophysical Journal International, **129**, 477–494.

Zimmerman, R., and I. Main, 2003, Hydromechanical behavior of fractured rocks, *in* Mechanics of Fluid-Saturated Rocks: Elsevier, 363–421.

LIST OF FIGURES

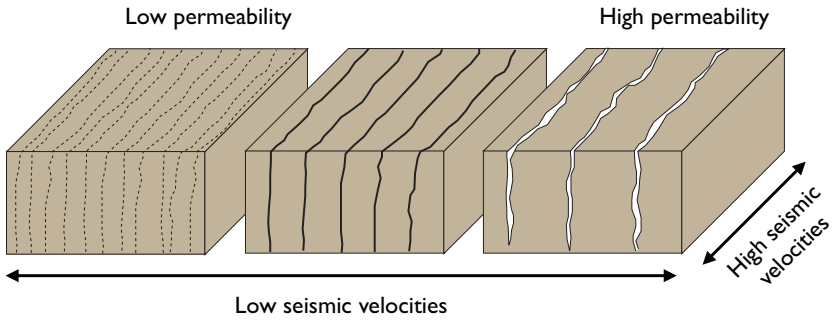

Figure 1: Schematic diagram showing the effect of oriented fracture sets on seismic and permeability anisotropy. The effect of fractures on seismic velocities is ambiguous, as the same anisotropy can be caused by a large number of small stiff fractures or a smaller number of open compliant fractures. Fluid flow, however is dominated by large fractures, so the models are expected to have different permeability anisotropy.

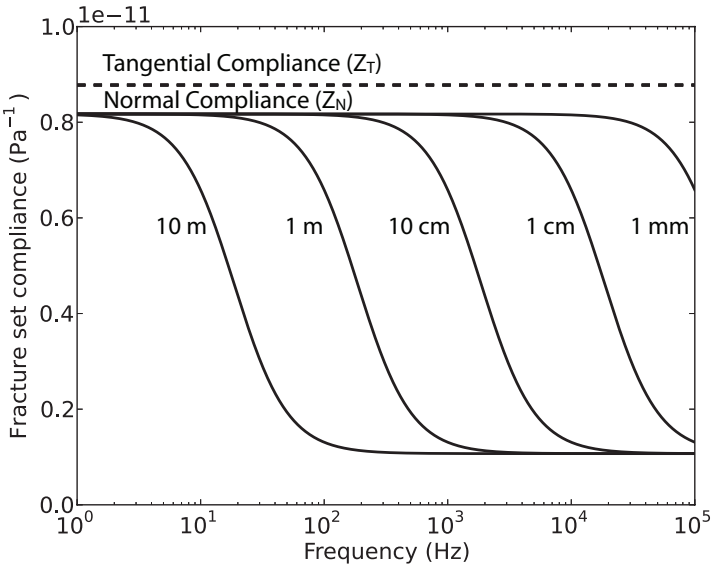

Figure 2: Predicted normal (solid line) and tangential (dashed line) fracture compliances as a function of frequency for different fracture sizes using the squirt-flow model of (Chapman, 2003). Tangential compliance shows no frequency dependence, while normal compliance decreases with increasing frequency. The frequency band where the change occurs, is highly sensitive to the fracture size. See appendix A for details of how these are calculated.

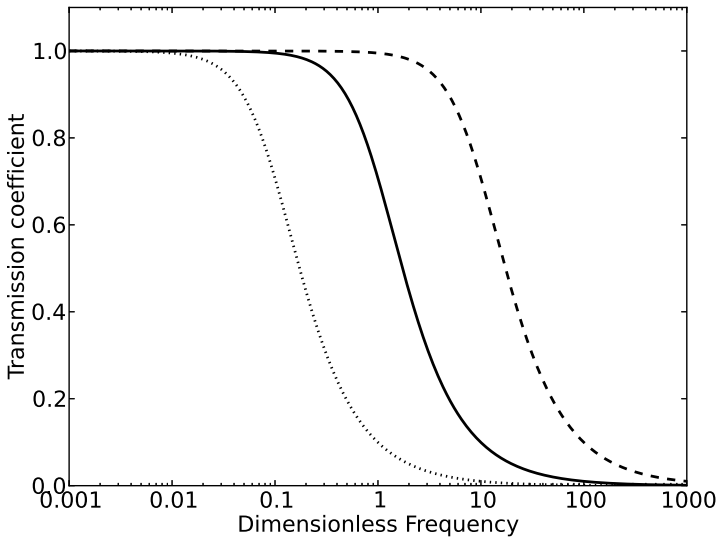

Figure 3: Predicted transmission coefficient ($|T|$, equation 5) as a function of dimensionless frequency ($\omega\rho V_{P,S}B_{N,T}/2$) for a wave propagating normal to a fracture (solid line). Dotted and dashed lines indicate transmission coefficients for fractures an order of magnitude more complaint and less compliant, respectively. For a fracture with heterogeneous compliance there will be a frequency range where compliant portions will backscatter energy while stiffer portions continue to transmit it. The transmitted wave will only sample the stiffer portions of the fracture leading to an apparent frequency dependent compliance.

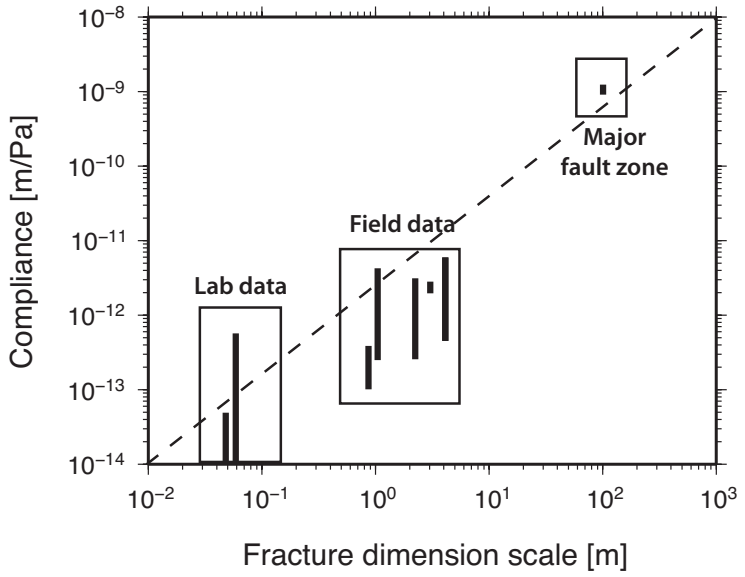

Figure 4: Laboratory and field estimates of fracture compliance as a function of fracture size. From the compilations of Worthington and Lubbe (2007), Hobday and Worthington (2012) and an additional measurement from Verdon and Wüstefeld (2012).

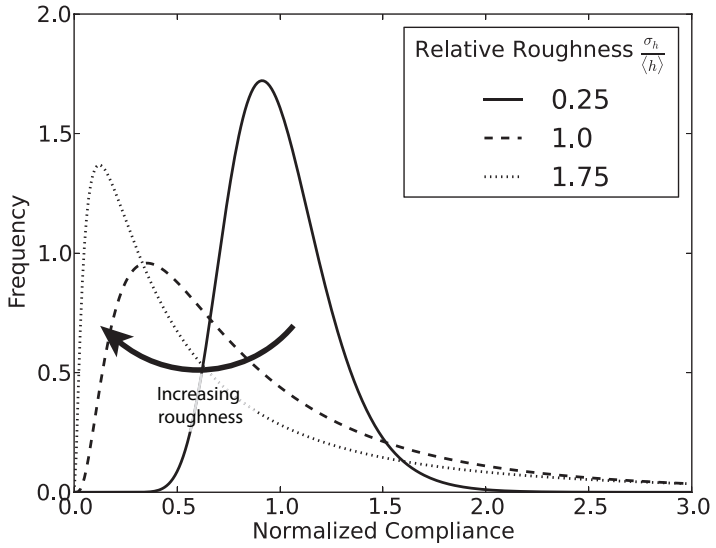

Figure 5: Predicted log-normal compliance distributions (equation 12) for different values of relative roughness $\left(\frac{\sigma_h}{\langle h \rangle}\right)$. For low roughness the distribution is approximately normal, but as roughness increases the distribution becomes increasingly skewed towards lower compliance, but with a long tail.

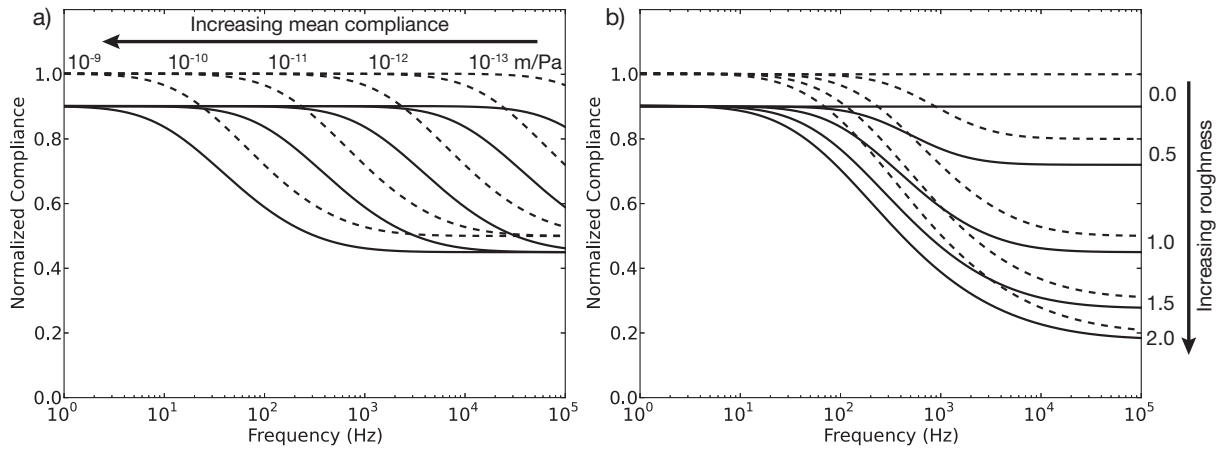

Figure 6: a) Predicted frequency dependent normal (B_N, solid) and tangential (B_T, dashed) compliances due to scattering for various values of mean tangential compliance (B_{T0}), using a relative roughness of 1.0. b) Predicted frequency dependent compliances for different values of relative roughness, using a B_{T0} of 10^{-10} m/Pa. Apparent compliances are calculated with equation 10 using transmission coefficients from equation 15, B_{N0}/B_{T0} is assumed to be 0.9. Compliances are normalized by B_{T0}.

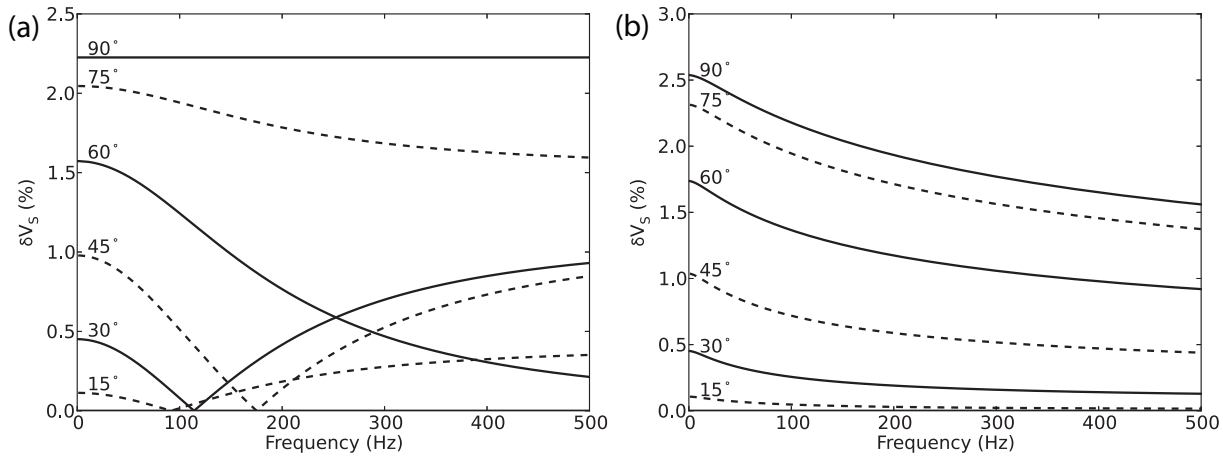

Figure 7: Predicted shear wave splitting for (a) the squirt-flow model, and (b) the scattering model as a function of frequency for different wave propagation directions relative to the fracture normal direction. Solid and dashed lines alternate for successive ray azimuths for clarity. Both models show the greatest magnitude of splitting for waves propagating parallel to the fracture (90°), however since these waves are only affected by tangential compliance the squirt-flow model shows no frequency dependence. For other propagation directions the normal compliance also plays a role and frequency dependence is observed for both models. Details for model parameters are given in the text.

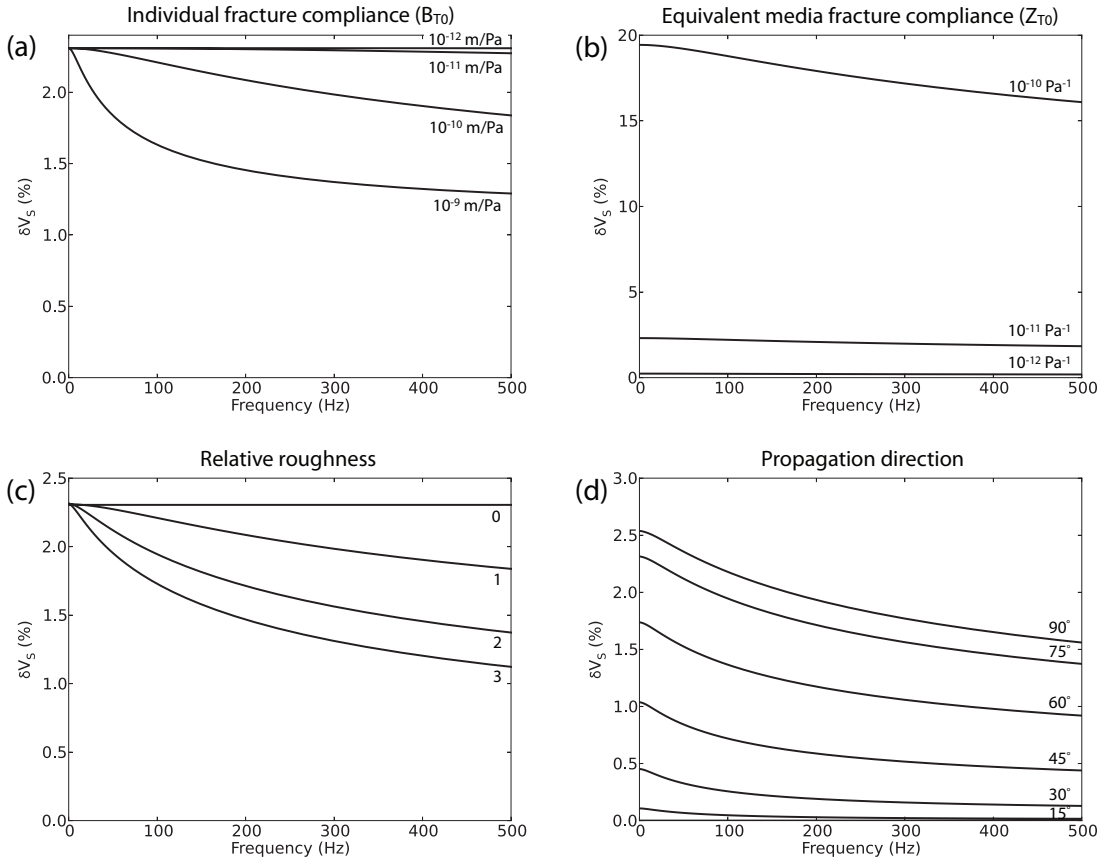

Figure 8: Predicted frequency dependent shear-wave splitting for the scattering model, showing sensitivity of the input parameters.

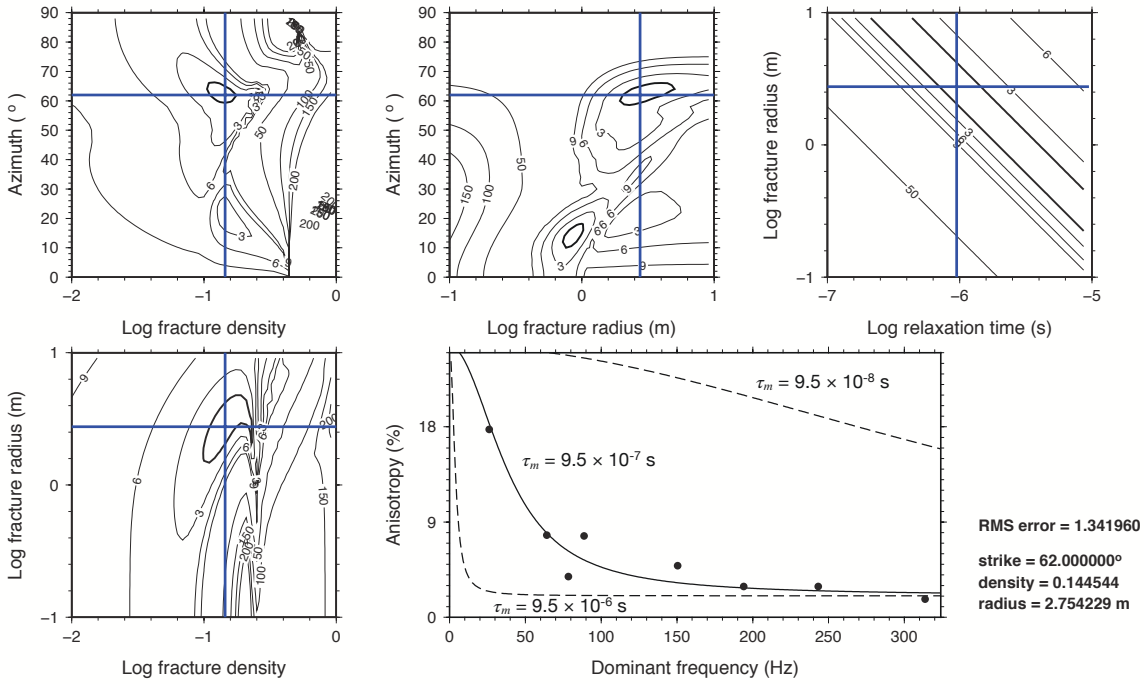

Figure 9: Inverted frequency dependent shear wave splitting data from a fractured limestone reservoir using the squirt-flow mechanism. Solid line shows best fit model from (Al-Harrasi et al., 2011b), which assumed a relaxation time of $\tau_m = 9.5 \times 10^{-7}$ s, and yielded a fracture radius, a_f, of 2.75 m a fracture density of 0.145 with the ray path traveling approximately 60° from the fracture normal. The misfit plot between fracture radius and relaxation time highlights the large tradeoff between the accuracy of these parameters. Dashed lines show the same model but with τ_m increased and decreased by an order of magnitude.

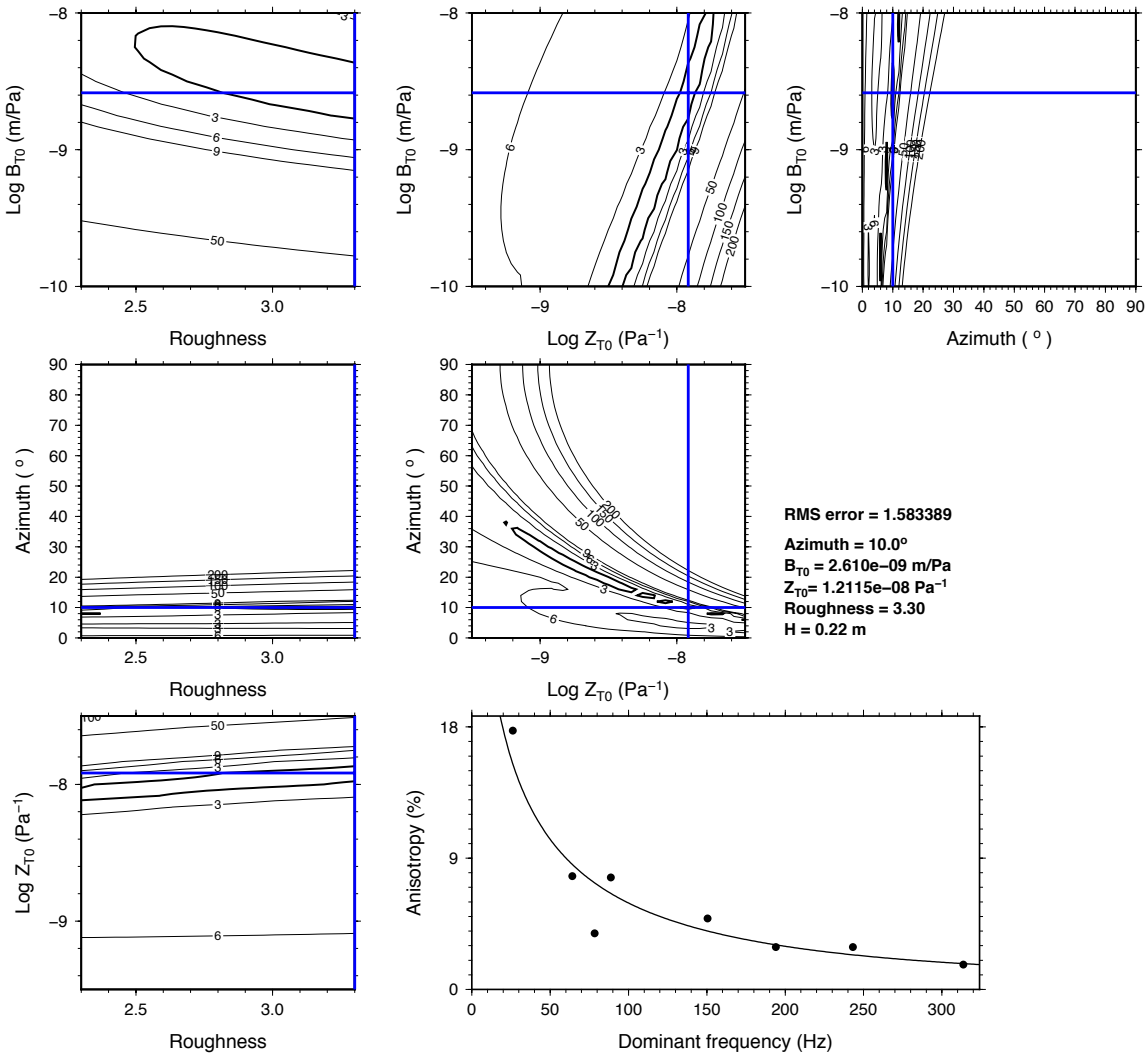

Figure 10: Inversion of frequency dependent shear wave splitting data using the scattering mechanism. The grid searches over wave azimuth (0° fracture normal, 90° fracture parallel), fracture roughness, mean fracture compliance (B_{T0}), and mean effective-media compliance (Z_{T0}). The thick contour shows the 90% confidence interval. The blue lines indicate the best fitting fracture parameters. The bottom right plot shows the observed data (dots) and the best fitting modeled results (line). Although the model does provide a good fit, the inverted roughness and B_{T0} are much higher than would be reasonably expected for reservoir fractures.

LIST OF TABLES

Table 1: List of symbols used in the models

Symbol	Description	Unit
Z_N, Z_T	Normal and Tangential effective media compliances of fracture sets	Pa^{-1}
B_N, B_T	Normal and Tangential Individual fracture compliances	m/Pa
	Squirt-flow model parameters	
τ_m, τ_f	mineral-scale and fracture-scale relaxation time	s
ζ	Average grain size	m
a_f	Average fracture size	m
	Scattering model parameters	
B_{N0}, B_{T0}	Mean low-frequency individual fracture compliances	m/Pa
$\frac{\sigma_h}{\langle h \rangle}$	Relative roughness parameter	dimensionless
H	Average fracture spacing	m